Chemical Science

Accepted Manuscript

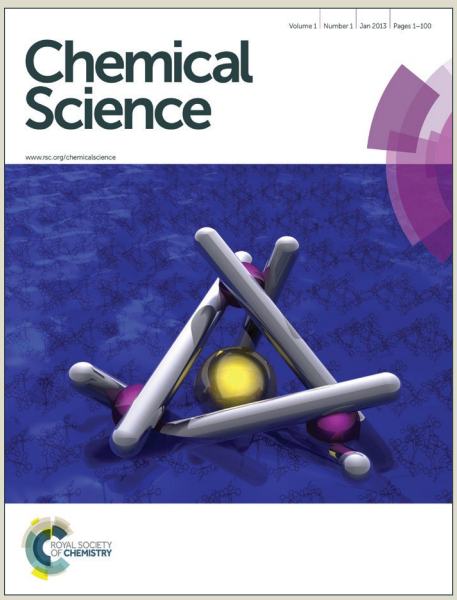

ROYAL SOCIETY OF CHEMISTRY

www.rsc.org/chemicalscience

Journal Name

ARTICLE

Tailor-made Porosities of Fluorene-based Porous Organic Frameworks for Pre-designable Fabrication of Palladium Nanoparticles with Size, Location and Distribution Control

Received 00th January 20xx,
Accepted 00th January 20xx

DOI: 10.1039/x0xx00000x

www.rsc.org/

Hong Zhong, Caiping Liu, Yangxin Wang, Ruihu Wang,* Maochun Hong

ABSTRACT Porous organic frameworks (POFs) are a new class of promising supports for metal nanoparticles (NPs), the size, location and distribution of metal NPs are closely related to porous nature of POFs. In this contribution, three fluorene-based POFs containing coordination-inert hydrogen, propyl and benzyl substituents at 9-position of fluorene units (POF-1, POF-2 and POF-3) were synthesized through simple click reaction. The substituents have exerted important influences on surface area, pore volume and pore size of POFs. Palladium NPs with pre-designable size, location and distribution were synthesized through the substituent-controlled strategy. When POF-1 was employed as a support, ultrafine palladium NPs in the interior pores were generated, while the introduction of propyl at 9-position of fluorene in POF-2 gave rise to a dual-distributed palladium NPs in the interior pores and on the external surface. The use of bulkier benzyl substituent resulted in the formation of palladium NPs on the external surface of POF-3. Hydrogenation of olefins has demonstrated that palladium NPs on the external surface possessed higher catalytic activity, while palladium NPs in the interior pores exhibited higher stability and recyclability. In addition, after Pd/POF-1, Pd/POF-2 and Pd/POF-3 were stored in air over half year, palladium NPs in the interior pores showed negligible change in comparison with fresh samples, while an obvious agglomeration was observed for palladium NPs on the external surface.

Introduction

Porous organic frameworks (POFs) have attracted considerable interest in gas storage, drug delivery, sensing and heterogeneous catalysis owing to their large surface area, flexible synthetic strategy and high stability.[1-5] They can serve as promising supports for metal nanoparticles (NPs) based on their powerful confinement effects. Metal NPs are usually encapsulated in the interior pores or dispersed on the external surface, or dually distributed on the external surface and in the interior pores of POFs.[6-10] A variety of approaches including the introduction of coordination groups[11-14] and judicial selection of reductive method of metal precursors[15] have been developed, but metal NPs with pre-designable size, location and distribution are still not predictably fabricated. The controllable synthesis of metal NPs is regarded as one of priorities for developing highly efficient catalytic systems and is inevitably tied to the search of new supports with unique structures and properties.[16-18] Therefore, it is a great challenge to establish a general and facile POFs platform, which allows to flexibly adjust size, location and distribution of metal NPs immobilized by POFs.

As well known, the properties of metal NPs are closely related to porous nature of POFs, one of feasible solutions for tailor-made porosities of POFs is the use of the strategy of post-synthetic modification.[19-28] Recently, Zhu *et al.* have adjusted pores of cationic POFs through changing size of the exchanged anions for selective adsorption of gas molecules.[24] Zhou *et al.* have modified POFs using alkyl amino and sulfate groups to increases gas adsorption ability.[25,26] Jiang *et al.* have accomplished the functionalization of surface pores by facile click reaction between azides and alkynes.[27,28] However, their applications have mainly focused on gas sorption and separation, the exploration of supporting metal NPs for heterogeneous catalysis is seldom reported. In addition, random incorporation of the introduced groups is unfavorable for precisely tuning size, location and distribution of metal NPs.[29,30] In contrast, the modification of building units of POFs at molecular level is more reliable to modulate pore size and surface properties, moreover, the inherent electronic and steric properties of the introduced groups may deliberately balance the interactions between POFs and metal NPs, and finally endowing metal NPs unique physicochemical and catalytic properties.[31-33] The selection of the modifiable building units is crucial for the construction of POFs with

State Key Laboratory of Structural Chemistry, Fujian Institute of Research on the Structure of Matter, Chinese Academy of Sciences, Fuzhou, Fujian 350002, China, E-mail: ruihu@fjirsm.ac.cn.

Electronic supplementary information (ESI) available: Detailed experimental materials, general synthetic procedures for the building blocks and the polymer frameworks; TGA, FT-IR spectra, solid state NMR spectra, SEM images, additional gas adsorption data, and theoretical calculation. See DOI: 10.1039/x0xx00000x

optimal porous natures. Although the tune of surface area, pore volume and pore size of POFs has been achieved through varying length of organic linkages and selecting suitable synthetic methods,[34-39] it is still imperative to develop a general and systematic method of tailor-made porosities for establishing well-defined relationship between porosities of POFs and the supported palladium NPs.

As a kind of distinctive electron-rich aromatic compounds, fluorene possesses attractive characteristics of structural modification, it is ready to polymerize at the positions of 2 and 7 through various chemical reactions, while the functionalization at the 9-position may modify properties of the resulting polymers for a specific purpose.[40-45] Many fluorene-based supramolecular architectures and optoelectronic materials have been presented,[41,44] but the application of fluorene-based POFs as stabilizers of metal NPs has not been reported hitherto. Herein, we chose the 9-position-substituted fluorene as monomers, and presented three fluorene-based POFs containing coordination-inert hydrogen, propyl and benzyl substituents (POF-1, POF-2 and POF-3), the synthesis of size, location and distribution of palladium NPs in POFs were achieved for the first time by tailoring porous nature of POFs using the substituent-controlled strategy.

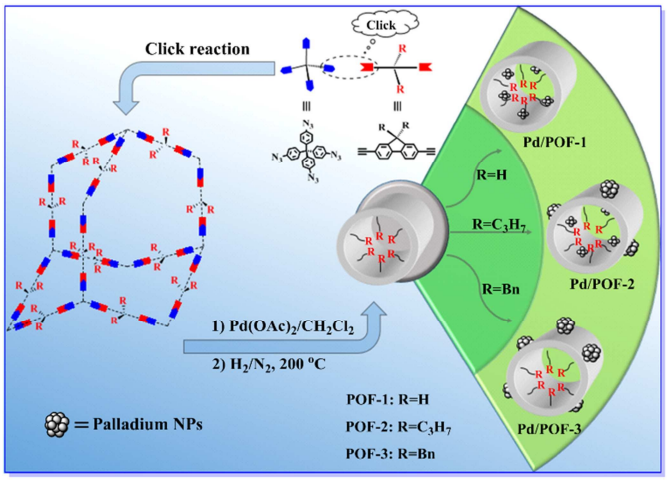

Scheme 1 Schematic synthesis of POF-1, POF-2, POF-3, Pd/POF-1, Pd/POF-2 and Pd/POF-3

Results and discussion

POF-1, POF-2 and POF-3 were readily prepared by click reactions between tetrakis(4-azidophenyl)methane and 9-position-substituted 2,7-diethynylfluorene (R = H, propyl and benzyl) under the standard click conditions (Scheme 1). After the reaction, the precipitates were collected by filtration and washed successively with aqueous EDTA-2Na solution, ethanol and CH_2Cl_2 to remove any possible residues. The resultant deep yellow powders were further treated by Soxhlet extraction in CH_2Cl_2 and dried *in vacuo* at 80 °C for 12 h.

POF-1, POF-2 and POF-3 are stable in water and air atmosphere, their structures and compositions were defined by FTIR, solid-state ^{13}C NMR and elemental analysis. In FTIR spectra (Figure S1), the characteristic peaks of azido at 2121 cm^{-1} and terminal alkynyl around 3280 and 2100 cm^{-1} totally disappear, the concomitant appearance of N=N stretching vibration peak around 1607 cm^{-1} demonstrates the formation of 1,2,3-triazolyl linkage.[46-48] Solid state ^{13}C NMR spectra further indicate the presence of 1,2,3-triazolyl linkage by the resonance of C4-triazolyl carbon at 148 ppm (Figure S2).[11,46] The broad signals at 145~120 and 65 ppm correspond to the aromatic carbon atoms and the central carbon of the tetraphenyl-methane core, respectively.[32,49] The peak at 36 ppm is assigned as the 9-positioned carbon atom of fluorene units in POF-1, while the peak in POF-2 and POF-3 is shifted to 54 and 56 ppm, respectively, owing to the introduction of propyl and benzyl substituents. The other peaks at 58~13 ppm in POF-2 and POF-3 may be ascribed to the alkyl carbon atoms of substituents. In TGA curves of POF-1, POF-2 and POF-3, the initial weight losses of 5.3, 5.1 and 2.0 % before 115 °C were observed, respectively (Figure S3), XRD analyses reveal they are amorphous due to kinetic irreversibility of click reaction (Figure S4).[50] A granular morphology with particle diameter of 20-50 nm was observed in their SEM images (Figure S5).

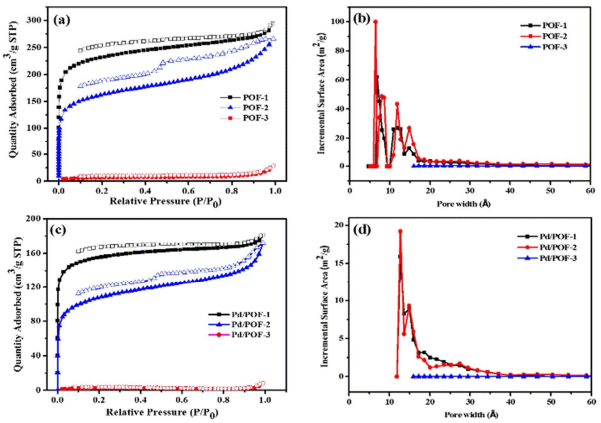

Fig. 1 Nitrogen adsorption/desorption isotherms (a, c) and pore size distribution (b, d) for POF-1, POF-2, POF-3, Pd/POF-1, Pd/POF-2 and Pd/POF-3.

The porosities of POF-1, POF-2 and POF-3 were investigated by physisorption of nitrogen at 77 K (Figure 1a). The rapid nitrogen uptake at very low relative pressure ($P/P_0 < 0.01$) suggests the presence of extensive micropores in POF-1 and POF-2, while the uptake in POF-3 is negligible due to pore filling by bulky benzyl groups.[51-53] An obvious hysteresis and step ($P/P_o = 0.46$) were observed in the desorption isotherm of POF-2 owing to the interspersion of propyl group in the micropores.[26] BET surface area and total pore volume in POF-1 are 871 $m^2\ g^{-1}$ and 0.43 $cm^3\ g^{-1}$, respectively, which are decreased to 622 $m^2\ g^{-1}$ and 0.30 $cm^3\ g^{-1}$, respectively, in POF-2 (Table S1). The pore size distribution reveals that the predominant pores in POF-1 and POF-2 are in the microporous range (Figure 1b). In contrast, POF-3 shows negligible BET surface area of 23 $m^2\ g^{-1}$ and no significant micropores were detected because two benzyl groups at 9-position of fluorene

units lead to the loss of the pores. H_2 adsorption capacities were also investigated at 77 K and 1 bar. As shown in Figure S6a, POF-1 and POF-2 exhibits high H_2 uptake of 115 and 103 cm^3 g^{-1}, respectively, due to their dominant microporous structure.[54] Interestingly, H_2 uptake of POF-3 is 31 cm^3 g^{-1} despite of its negligible BET surface area. In addition, an obvious hysteresis was observed in POF-3.

Considering the important role of substituents in modulating porous structures of POFs, their influences on palladium NPs were further investigated. The treatment of POF-1, POF-2 and POF-3 with $Pd(OAc)_2$ in a 2:1 molar ratio of triazoly to palladium in CH_2Cl_2, and subsequent reduction in a stream of H_2/N_2 gave rise to Pd/POF-1, Pd/POF-2 and Pd/POF-3, respectively. Palladium contents in Pd/POF-1, Pd/POF-2 and Pd/POF-3 are 0.31, 0.43 and 0.61 mmol g^{-1}, respectively. Notably, when the usage amount of $Pd(OAc)_2$ is doubled for POF-1 under other identical conditions, palladium content of 0.33 mmol g^{-1} is similar to that in Pd/POF-1, which suggests that palladium loading is governed by the porosities of POFs. FTIR, (Figure S1) solid-state ^{13}C NMR (Figure S2) and SEM (Figure S5) spectra of Pd/POF-1, Pd/POF-2 and Pd/POF-3 are almost identical with that of POF-1, POF-2 and POF-3, respectively, indicating their structural frameworks are well maintained after palladium loading.[11] The thermal stability of Pd/POF-1, Pd/POF-2 and Pd/POF-3 are lower than that of POF-1, POF-2 and POF-3, respectively (Figure S3). In their XRD patterns, no obvious characteristic peaks of palladium NPs were observed (Figure S4). The shapes of N_2 adsorption/desorption isotherms (Figure 1c) in Pd/POF-1, Pd/POF-2 and Pd/POF-3 are preserved in comparison with their original frameworks, indicating that the pore systems have not been altered substantially after supporting palladium NPs.[8] BET surface areas of Pd/POF-1, Pd/POF-2 and Pd/POF-3 are decreased to 588, 438 and 9 m^2 g^{-1}, respectively, owing to partial pore filling and/or mass increment after palladium loading. It should be mentioned that the pore sizes less than 10 Å almost disappear in Pd/POF-1 and Pd/POF-2 (Figure 1d). H_2 uptake amounts of Pd/POF-1, Pd/POF-2 and Pd/POF-3 are slightly decreased to 104, 90 and 28 cm^3 g^{-1}, respectively (Figure S6b).

Transmission electron microscope (TEM) images clearly show that ultrafine palladium NPs in Pd/POF-1 are uniformly encapsulated in the interior pores of POF-1, and their average size is 1.60±0.40 nm (Figure 2a-c), which is small enough to be accommodated by the interior cavities of POF-1. In contrast, palladium NPs in Pd/POF-2 exhibit a dual size distribution. The relatively small palladium NPs with an average diameter of 2.15±0.45 nm are located in the interior pores of POF-2, while large NPs with an average diameter of 3.65±0.45 nm are deposited on the external surface of POF-2 (Figure 2d-f). Interestingly, palladium NPs in Pd/POF-3 are uniformly dispersed on the external surface of POF-3 due to the absence of micropores, which are stabilized by both coordination interaction of surface 1,2,3-triazolyl and π interaction of flexible benzyl groups. The average size of palladium NPs in Pd/POF-3 is 3.55±0.65 nm (Figure 2g-i), which is close to that on the external surface of POF-2. HAADF-STEM further confirms the size, location and distribution of palladium NPs in Pd/POF-1, Pd/POF-2 and Pd/POF-3 (Figure 2c,f,i).

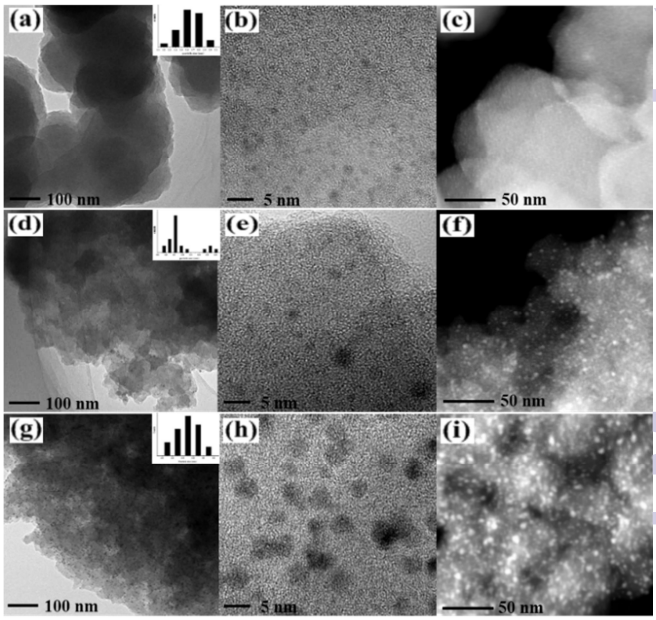

Fig. 2 TEM and HAADF-STEM images of palladium NPs for Pd/POF-1 (a, b, c), Pd/POF-2 (d, e, f), and Pd/POF-3 (g, h, i).

It has been reported that the usage amount of palladium precursors may affect the size, location and distribution of palladium NPs,[55,56] however, no significant change in TEM images of Pd/POF-1 was observed when two times amount of $Pd(OAc)_2$ was used under the same conditions (Figure S7), which further indicates palladium NPs are closely associated with pore nature of POFs.

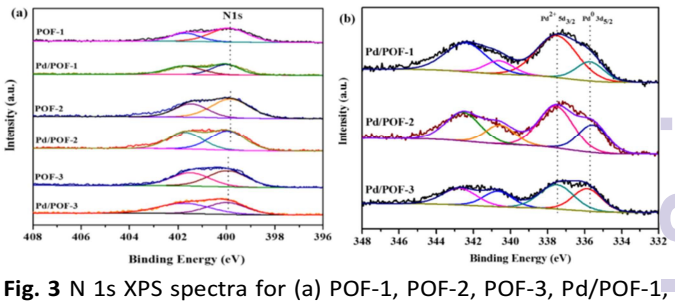

Fig. 3 N 1s XPS spectra for (a) POF-1, POF-2, POF-3, Pd/POF-1, Pd/POF-2 and Pd/POF-3; (b) Pd 3d XPS spectra of Pd/POF-1, Pd/POF-2 and Pd/POF-3.

X-ray photoelectron spectroscopy (XPS) of POF-1, POF-2 and POF-3 are shown in Figure S8, the binding energy peaks at 284.8 and 399.8 eV correspond to C 1s and N 1s, respectively. The N 1s region is divided into two peaks. One peak at 401.5 eV corresponds to N2 atom of 1,2,3-triazolyl, the other peak at 399.8 eV may be assigned to N1 and N3 atoms, and the ratio of their relative peak areas is ~1:2 (Figure 3a), which further confirms the formation of 1,2,3-triazolyl linkage.[50] In order to clarify the interaction between the supports and the incorporated palladium species, N1s XPS spectra of Pd/POF-1,

Pd/POF-2 and Pd/POF-3 were investigated (Figure 3a). The binding energy peaks of N 1s positively shift by 0.35, 0.25 and 0.05 eV, respectively, in comparison with their respective POFs, indicating that the interaction between the supports and palladium NPs gradually weakens when the substituents change from hydrogen to propyl to benzyl. The existing states of surface palladium in Pd/POFs were also investigated by XPS (Figure 3b). Pd 3d region is divided into two spin-orbital pairs, indicating that there are two types of the surface-bound palladium species.[7] For Pd/POF-1, the binding energy peaks at 335.75 (Pd $3d_{5/2}$) and 340.65 eV (Pd $3d_{3/2}$) are assigned to Pd(0) species, while the peaks at 337.55 (Pd $3d_{5/2}$) and 342.45 eV (Pd $3d_{3/2}$) correspond to Pd(II) species. The presence of Pd(II) species is probably ascribed to the residual palladium acetate and/or reoxidation of Pd(0) during air contact.[50] A comparison of relative peak areas of Pd(0) and Pd(II) shows that the ratio of Pd(0) to Pd(II) is 0.31. The Pd $3d_{5/2}$ binding energy peaks of Pd(0) species in Pd/POF-2 and Pd/POF-3 are 335.60 eV and 336.05, respectively. In comparison with that in Pd/POF-1, the negative shift by 0.15 eV in Pd/POF-2 and positive shift by 0.30 eV in Pd/POF-3 may be ascribed to the inductive effect of electron-donating propyl and electron-withdrawing benzyl, respectively, resulting in more electron-rich Pd(0) species in Pd/POF-2 and electron-deficient Pd(0) species in Pd/POF-3. The ratios of Pd(0) to Pd(II) in Pd/POF-2 and Pd/POF-3 are 0.56 and 0.78, respectively. The gradually increased ratios of Pd(0) to Pd(II) are consistent with the distribution trends of palladium NPs from the interior pores to the external surface. These observations further reveal that porous nature of POFs has an important influence on palladium NPs.

To have a clear insight into the influences of substituents on electronic properties of POFs and the interactions between POFs and palladium NPs. Density functional theory (DFT) calculations were performed based on POFs and Pd/POFs model compounds. As shown in Table S2, hydrogen, propryl and benzyl substituents of fluorene units have negligible influence on the bond distances, but they slightly affect the dihedral angles of N_2-N_1-N_4-N_5 (θ) and the angles between pseudo-planes of Pd/POFs (τ). The nitrogen atoms of 1,2,3-triazolyl in both POFs and Pd/POFs possess negative charge, but N1 atom is more negative than N2 and N3, which demonstrates that N1 possesses more charge density and prefers to coordinate with palladium (Figure S9), which is the same as those in the click-based coordination compounds.[8] Notably, the charge of N1 in Pd/POFs is more negative than that in POFs, while the charges of N2 and N3 in Pd/POFs are more positive than those in POFs, indicating that the electron transfer from N2 and N3 to N1 after palladium loading. The charges of fluorene units in POF-1 and Pd/POF-1 are 0.00373 and 0.00363 *e*, respectively. The introduction of propyl and benzyl substituents results in slightly negative and positive shifts, respectively (Table S3), which are consistent with the results of their XPS analyses. The highest occupied molecular orbital (HOMO) and the lowest unoccupied molecular orbital (LUMO) in POFs are shared by triazolyl and fluorene units owing to their conjugative effect. However, HOMOs in Pd/POFs are mainly occupied by palladium species, and LUMOs are shared by triazolyl and fluorene units (Figure S10).

To understand the roles of size, location and distribution of palladium NPs in catalytic reactions, Pd/POF-1, Pd/POF-2 and Pd/POF-3 were initially evaluated by solvent-free hydrogenation of styrene under 25 °C and 1.0 atm H_2. As shown in Figure 4a, Pd/POF-1 afforded a full conversion of styrene to phenylethane in 5 h, while the use of Pd/POF-3 gave a complete conversion in 3 h under the same conditions. As expected, the catalytic activity of Pd/POF-2 was in the middle of Pd/POF-1 and Pd/POF-3 owing to dual size distribution of palladium NPs in the interior pores and on the external surface (Figure 2). The highest catalytic activity of Pd/POF-3 is probably attributed to the improvement of mass transport and easy availability of active sites on the external surface. As comparison, commercial Pd/C was also tested under the same conditions, and a complete conversion of styrene was achieved in 4 h, which is inferior to that of Pd/POF-3.

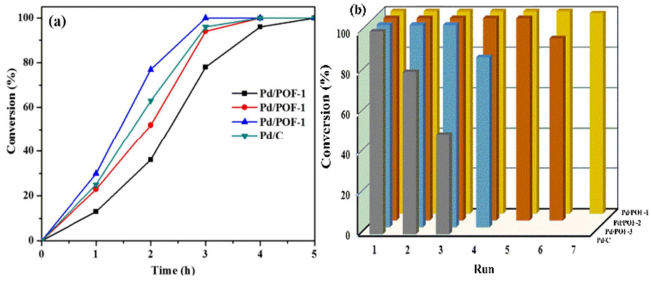

Fig. 4 (a) The conversion of styrene as a function of time in hydrogenation reactions. (b) Recyclability for Pd/POF-1 Pd/POF-2, Pd/POF-3 and Pd/C. Reaction condition: styrene (2 mL, 21 mmol), [Pd] (0.02 mol %), 1.0 atm of H2, 25 °C, 6 h.

Besides activity, other important factors for a hererogeneous catalytic system, such as recyclability and stability, were also examined. As shown in Figure 4b, Pd/POF-1 could be used at least 7 runs with 100 % conversion of styrene, while 90 and 83% conversions were achieved after the hydrogenation reactions of Pd/POF-2 and Pd/POF-3 were performed for six runs and four runs, respectively. In contrast, Pd/C afforded 80 and 49 % conversions of styrene in the second and third runs, respectively.

To explore stability of palladium NPs in these catalytic systems, the black powders were isolated after consecutive reactions and were examined by TEM. As shown in Figure 5, the majority of palladium NPs in Pd/POF-1-7run are in the interior pores of the host framework, the average size of palladium NPs is slightly increased to 2.0 nm. However, a few palladium NPs diffuse out the micropores, and aggregate on the external surface of POF-1 (Figure 5a, b), which is consistent with the reported NPs encapsulated in the interior pores of POFs.[8,11] Interestingly, palladium NPs in Pd/POF-2-6run maintain their dual size distribution, the average size of palladium NPs in the interior pores and the external surface are increased from 2.15 to 2.50 nm and from 3.65 to 6.50 nm, respectively (Figure 5c, d). For Pd/POF-3, an obvious agglomeration was observed after the fourth runs (Figure 5e,

f). The superior stability of palladium NPs in the interior cavities of POF-1 probably result from the confinement interaction of host frameworks and the coordination interaction of 1,2,3-triazoyl linkage. However, the coordination interaction of 1,2,3-triazolyl and π interaction of benzyl ring are not enough to efficiently immobilize palladium NPs on the external surface of POF-3, resulting in deactivation and the loss of catalytic activity after consecutive reaction. ICP analyses demonstrate palladium leaching after the first run hydrogenation of Pd/POF-1, Pd/POF-2 and Pd/POF-3 is 0.76, 1.41 and 2.09 ppm, respectively, which is agreement with the stability of palladium NPs.

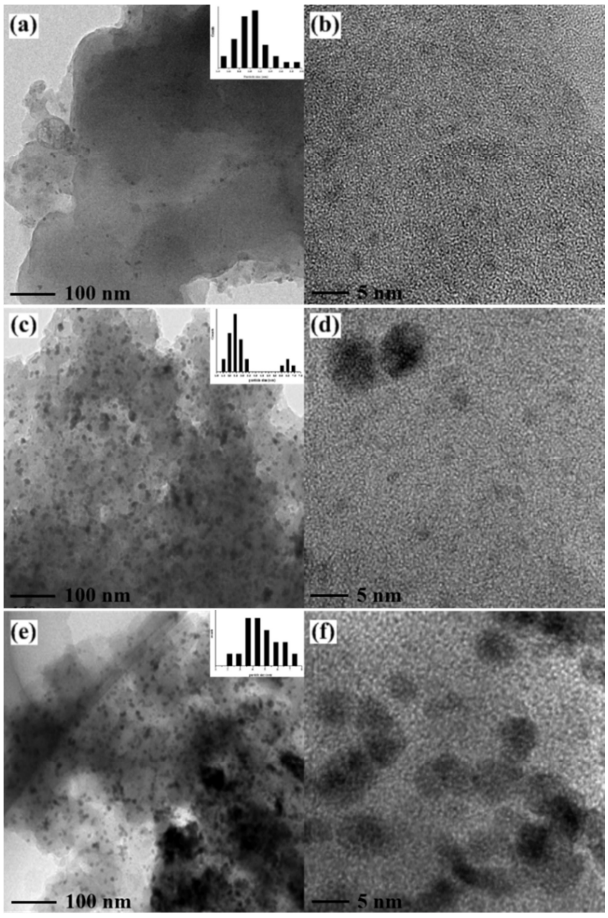

Fig. 5 TEM images for Pd/POF-1-7run (a, b), Pd/POF-2-6run (c, d) and Pd/POF-3-4run (e, f).

The stability of Pd/POF-1, Pd/POF-2 and Pd/POF-3 were also examined after they were stored in air over half year. As shown in Figure S11, the size, location and distribution of palladium NPs in Pd/POF-1 have no significant change in comparison with fresh sample, However, the average size of palladium NPs on the external surface of Pd/POF-2 increases to 4.50 nm, and an obvious agglomeration of palladium NPs was observed in Pd/POF-3, which further reveals that palladium NPs encapsulated in the interior pores of POFs possess higher stability than those deposited on the external surface.

The outstanding catalytic recyclability and stability of Pd/POF-1 in hydrogenation of styrene encouraged us to explore generality of the catalytic system. As shown in Table 1, hydrogenation of styrene afforded a 100 % GC yield under 1.0 atm H_2 at 25 °C for 6 h (entry 1), while no target product was detected when the control experiment was performed in the presence of only POF-1 (entry 2). When $Pd(OAc)_2$ supported by POF-1 was used as a catalyst, only trace amount of phenylethane was formed (entry 3). A series of chain-, cyclo- and phenyl-olefins were also tested under the same conditions. The use of linear 1-hexene and 1-octene generated the corresponding products in quantitative yields in 6 h (entries 4 and 5). Interestingly, hydrogenation of cyclohexene also gave rise to the target product in a quantitative yield in 6 h (entry 6). The catalytic system was also effective for hydrogenation of 1,4-cyclohexadiene. The target product was obtained in 100 % conversion and 77 % cyclohexane selectivity in 6 h (entry 7), complete hydrogenation to cyclohexane was achieved when reaction time was prolongated to 12 h (entry 8). Notably, after hydrogenation of styrene was run for 1 h, the palladium-containing catalytic species were quickly removed by filtration, and the filtrate was continued to react for the additional 11 h, and a negligible change in conversion was observed (entries 9 and 10), which indicates that hydrogenation proceeds in a heterogeneous manner in the catalytic system. The catalytic activity of palladium NPs was also examined after they were stored in air over half year. In comparison with fresh samples, no significant change was observed for the stored Pd/POF-1 and Pd/POF-2 (entries 11 and 12). However, the conversion for the stored Pd/POF-3was decreased to 86% (entry 13).

Table 1. Hydrogenation of olefins[a]

Entry	olefins	Time (h)	Con. (%)[b]	Sel. (%)
1	styrene	6	100	100
2[c]	styrene	6	0	0
3[d]	styrene	6	<3	100
4	1-hexene	6	100	100
5	1-octene	6	100	100
6	cyclohexene	6	100	100
7	1,4-cyclohexadiene	6	100	77
8	1,4-cyclohexadiene	12	100	100
9	styrene	1	15	100
10[e]	-	12	15	100
11[f]	styrene	6	100	100
12[g]	styrene	6	100	100
13[h]	styrene	6	86	100

[a] Hydrogenation was performed in olefins (2 mL) and [olefins (mol)/Pd (mol) = 5000] in 1.0 atm H_2 at 25 °C; [b] conversion and selectivity were determined by GC; [c] POF-1 was used in the absence of palladium; [d] $Pd(OAc)_2$/POF-1 was used as a catalyst; [e] filtration experiment; [f] Pd/POF-1 was stored over half year; [g] Pd/POF-2 was stored over half year; [h] Pd/POF-3 was stored over half year.

Conclusions

The porosities of POFs were modulated through varying coordination-inert substituents of fluorene-based building units at molecular level. These POFs can serve as effective supports for the synthesis of palladium NPs with tunable size, location and distribution by substituent-controlled strategy. To our knowledge, this is the first report for the synthesis of metal NPs through tailor-made porous properties of POFs. The surface area, pore volume and pore size in POFs have exerted important influences on palladium NPs and their catalytic performances. In Pd/POF-1, Pd/POF-2 and Pd/POF-3, the coordination interaction between supports and palladium NPs gradually weakens with concomitant increment of Pd(0) to Pd(II) ratios. Pd/POF-3 with palladium NPs on the external surface shows the highest catalytic activity in hydrogenation of olefins because of improvement of mass transport and easy availability of active sites, while Pd/POF-1 with ultrafine palladium NPs in the interior pores exhibits the highest stability and recyclability owing to the confinement effect of host frameworks and the coordination interaction of 1,2,3-triazoyl linkage. In summary, this study has established an appealing platform for pre-designable fabrication of metal NPs with size, location and distribution control using the substituent-controlled strategy, which opens a new and general avenue for synthesis of metal NPs immobilized by POFs. Further study will focus on the tunable synthesis of metal NPs with specific performances through molecular functionalization of modular building units in POFs.

Acknowledgements

This work was financially supported by the 973 Program (2011CBA00502) and the Natural Science Foundation (21273239 and 21471151) of China.

References

1 D. Wu, F. Xu, B. Sun, R. Fu, H. He and K. Matyjaszewski, *Chem. Rev.*, 2012, **112**, 3959-4015.
2 S. Kandambeth, D. B. Shinde, M. K. Panda, B. Lukose, T. Heine and R. Banerjee, *Angew. Chem. Int. Ed.*, 2013, **52**, 13052-13056.
3 L. Stegbauer, K. Schwinghammer and B.V. Lotsch, *Chem. Sci.*, 2014, **5**, 2789-2793.
4 X. Zou, H. Ren and G. Zhu, *Chem. Commun.*, 2013, **49**, 3925-3936.
5 Y. Zhang and S. N. Riduan, *Chem. Soc. Rev.*, 2012, **41**, 2083-2094.
6 J. F. Dienstmaier, A. M. Gigler, A. J. Goetz, P. Knochel, T. Bein, A. Lyapin, S. Reichlmaier, W. M. Heckl and M. Lackinger, *ACS Nano*, 2011, **5**, 9737-9745.
7 P. Pachfule, S. Kandambeth, D. D. Dıaz and R. Banerjee, *Chem. Commun.*, 2014, **50**, 3169-3172.
8 L. Li, H. Zhao, J. Wang and R. Wang, *ACS Nano.*, 2014, **8**, 5352-5364.
9 P. Pradip, K. P. Manas, K. Sharath, S. M. Shivaprasad, D. D. Rahul and D. Banerjee, *J. Mater. Chem. A.*, 2014, **2**, 7944-7952.
10 S. Y. Ding, J. Gao, Q. Wang, Y. Zhang, W. G. Song, C. Y. Su and W. Wang, *J. Am. Chem. Soc.*, 2011, **133**, 19816-19822.
11 H. Zhong, Y. Gong, F. Zhang, L. Li and R. Wang, *J. Mater. Chem. A.*, 2014, **2**, 7502-7508.
12 Q. Sun, M. Jiang, Z. Shen, Y. Jin, S. Pan, L. Wang, X. Meng, W. Chen, Y. Ding, J. Li and F. S. Xiao, *Chem. Commun.*, 2014, **50**, 11844-11847.
13 Q. Zhang, S. Zhang and S. Li, *Macromolecules.*, 2012, **45**, 2981-2988.
14 A. Saeed, F. Maya, D. J. Xiao, M. NajamulHaq, F. Svec and D. K. Britt, *Adv. Funct. Mater.*, 2014, **24**, 5790-5797.
15 J. F. V. Humbeck, T. M. McDonald, X. Jing, B. M. Wiers, G. Zhu and J. R. Long, *J. Am. Chem. Soc.*, 2014, **136**, 2432-2440.
16 Q. L. Zhu, J. Li and Q. Xu, *J. Am. Chem. Soc.*, 2013, **135**, 10210-10213.
17 Y. Z. Chen, Q. Xu, S. H. Yu and H. L. Jiang, *Small*, 2015, **11**, 71-76.
18 C. Wang, K. E. deKrafft and W. Lin, *J. Am. Chem. Soc.*, 2012, **134**, 7211-7214.
19 C. R. DeBlase, K. E. Silberstein, T. T. Truong, H. D. Abruña and W. R. Dichtel, *J. Am. Chem. Soc.*, 2013, **135**, 16821-16824.
20 P. Arab, M. G. Rabbani, A. K. Sekizkardes, T. İslamoğlu and H. M. El-Kaderi, *Chem. Mater.*, 2014, **26**, 1385-1392.
21 B. G. Hauser, O. K. Farha, J. Exley and J. T. Hupp, *Chem. Mater.*, 2013, **25**, 12-16.
22 S. Chakraborty, Y. J. Colon, R. Q. Snurr and S. T. Nguyen, *Chem. Sci.*, 2015, **6** , 384–389
23 D. Yuan, W. Lu, D. Zhao and H. C. Zhou, *Adv. Mater.*, 2011, **23**, 3723-3725.
24 Y. Yuan, F. Sun, L. Li, P. Cui and G. Zhu, *Nat. Commun.*, 2014, **5**, 4260-4267.
25 W. Lu, J. P. Sculley, D. Yuan, R. Krishna, Z. Wei and H. C. Zhou, *Angew. Chem. Int. Ed.*, 2012, **51**,7480-7884.
26 W. Lu, D. Yuan, J. Sculley, D. Zhao, R. Krishna and H. C. Zhou, *J. Am. Chem. Soc.*, 2011, **133**, 18126-18129.
27 A. Nagai, Z. Guo, X. Feng, S. Jin, X. Chen, X. Ding and D. Jiang, *Nat. Commun.*, 2011, **2**, 536-543.
28 F. Xu, H. Xu, X. Chen, D. Wu, Y. Wu, H. Liu, C. Gu, R. Fu and D. Jiang, *Angew. Chem. Int. Ed.*, 2015, **54**, 6814-6818.
29 F. M. Wisser, K. Eckhardt, D. Wisser, W. Bohlmann, J. Grothe, E. Brunner, S. Kaskel, *Macromolecules*, 2014, **47**, 4210-4216.
30 W. Wang, A. Zheng, P. Zhao, C. Xia and F. Li, *ACS Catal.*, 2014, **4**, 321-327.
31 R. Palkovits, M. Antonietti, P. Kuhn, A. Thomas and F. Schuth, *Angew. Chem. Int. Ed.*, 2009, **48**, 6909-6912.
32 Z. Xie, C. Wang, K. E. deKrafft and W. Lin, *J. Am. Chem. Soc.*, 2011, **133**, 2056-2059.
33 Y. Zhu, and W. Zhang, *Chem. Sci.*, 2014, **5**, 4957-4961.
34 N. B. McKeown and P. M. Budd, *Macromolecules*, 2010, **43** 5163-5176.
35 J. X. Jiang, F. Su, A. Trewin, C. D. Wood, N. L. Campbell, H. Niu, C. Dickinson, A. Y. Ganin, M. J. Rosseinsky, Y. Z. Khimyak and A. I. Cooper, *Angew. Chem. Int. Ed.*, 2007, **46**, 8574-8578.
36 Y. C. Zhao, T. Wang, L. M. Zhang, Y. Cui and B. H. Han, *ACS Appl. Mater. Interfaces*, 2012, **4**, 6975-6981.
37 D. B. Shinde, S. Kandambeth, P. Pachfule, R. R. Kumar and R. Banerjee, *Chem. Commun.*, 2015, **51**, 310-313.
38 K. V. Rao, R. Haldar, C. Kulkarni, T. K. Maji and S. J. George, *Chem. Mater.*, 2012, **24**, 969-971.
39 A. P. Cote, H. M. El-Kaderi, H. Furukawa, J. R. Hunt and O. M Yaghi, *J. Am. Chem. Soc.*, 2007, **129**, 12914-12915.
40 M. A. Karim, Y. R. Cho, J. S. Park, T. I. Ryu, M. J. Lee, M. Song, S. H. Jin, J. W. Lee and Y. S. Gal, *Macromol. Chem. Phys.*, 2008, **209**, 1967-1975.
41 C. Zhu, L. Liu, Q. Yang, F. Lv and S. Wang, *Chem. Rev.*, 2012, **112**, 4687-4735.
42 K. Y. Pu, K. Li, J. Shi and B. Liu, *Chem. Mater.*, 2009, **21**, 3816 3822.
43 B. B. Liu, T. T. T. Dan and G. C. Bazan, *Adv. Funct. Mater.*, 2007, **17**, 2432-2438.

44 K. Li, K. Y. Pu, L. Cai, B. Liu, *Chem. Mater.*, 2011, **23**, 2113-2119.
45 J. Song, Q. Yang, F. Lv, L. Liu and S. Wang, *ACS Appl. Mater. Interfaces*, 2012, **4**, 2885-2890.
46 P. Pandey, O. K. Farha, A. M. Spokoyny, C. A. Mirkin, M. G. Kanatzidis, J. T. Hupp and S. T. Nguyen, *J. Mater. Chem.*, 2011, **21**, 1700-1703.
47 J. R. Holst, E. D. Stockel, J. Adams and A. I. Cooper, *Macromolecules*, 2010, **43**, 8531-8538.
48 O. Plietzsch, C. I. Schilling, T. Grab, S. L. Grage, A. S. Ulrich, A. Comotti, P. Sozzani, T. Muller and S. Brase, *New J. Chem.*, 2011, **35**, 1577-1581.
49 A. Comotti, S. Bracco, M. Mauri, S. Mottadelli, T. Ben, S. Qiu and P. Sozzani, *Angew. Chem. Int. Ed.*, 2012, **51**, 10136-10140.
50 L. Li, C. Zhou, H. Zhao and R. Wang, *Nano Res*., 2015, **8**, 709-721.
51 S. Dalapati, S. Jin, J. Gao, Y. Xu, A. Nagai and D. Jiang, *J. Am. Chem. Soc.*, 2013, **135**, 17310-17313.
52 S. B. Kalidindi, H. Oh, M. Hirscher, D. Esken, C. Wiktor, S. Turner, G. V. Tendeloo and R. A. Fischer, *Chem. Eur. J.*, 2012, **18**, 10848-10856.
53 M. G. Rabbani, A. K. Sekizkardes, Z. Kahveci, T. E. Reich and R. Ding, *Chem. Eur. J.*, 2013, **19**, 3324-3328.
54 H. Oh, I. Savchenko, A. Mavrandonakis, T. Heine and M. Hirscher, *ACS Nano*, 2014, **8**, 761-770.
55 A. Aijaz and Q. Xu, *J. Phys. Chem. Lett.*, 2014, **5**, 1400-1411.
56 C. J. Liu, Y. Zhao, Y. Li, D. S. Zhang, Z. Chang and X. H. Bu, *ACS Sustainable Chem. Eng.*, 2014, **2**, 3-13.